

# Programmable Magnetic Tweezers and Droplet Microfluidic Device for High-Throughput Nanoliter Multi-Step Assays\*\*

Anaïs Ali-Cherif, Stefano Begolo, Stéphanie Descroix, Jean-Louis Viovy, and Laurent Malaquin\*

Droplet microfluidics offer unique capabilities for the development of high-throughput analytical systems.<sup>[1]</sup> It allows fluids to be aliquoted into volumes in the nanoliter or picoliter range, and then transported over arbitrary distances without dispersion or cross-contamination. Several droplet-based functions, such as merging,<sup>[2,3]</sup> splitting,<sup>[2]</sup> sorting,<sup>[2,4]</sup> or cell encapsulation,<sup>[3–5]</sup> have already been demonstrated. Moreover, thanks to their “pipeline” architecture, in which different samples follow the same track in a row, droplet microfluidics enable the implementation of high-throughput assays with relatively simple microfluidic designs, as compared for example, to systems in which the aliquoting is performed by valves integrated in the microfluidic system itself.<sup>[7]</sup>

Unfortunately, the ability to efficiently purify or extract molecules of interest from a complex matrix, a key component of most biochemical methods, is still missing from the functions currently available for droplet microfluidics. In macroscopic methods, the use of superparamagnetic beads as a solid state support has become very popular: they can bind an analyte of interest, be retained with a magnet while the supernatant fluid is removed, and release the analyte in an elution buffer. This process can be multiplexed, for example, using multiple magnets at the bottom of microtiter plates, but it still suffers from significant constraints, notably owing to 1) mass transfer limitations, 2) the need for relatively large volumes, and 3) poor mixing and washing efficiencies.

We already proposed an alternative approach, using self-assembled magnetic microcolumns in microfluidic format.<sup>[8,9]</sup> A large reduction in analysis time and increased automation was achieved in this way, but as with other microcolumn-based systems, this device does not allow for a high level of multiplexing and is not adapted to low-volume sample handling (that is less than 10  $\mu$ L). In this respect, the

combination of magnetic solid-phase extraction with droplet microfluidics is appealing. Magnetic-bead transfer between two droplets of several microliters was first introduced by Shikida et al.<sup>[10]</sup> Results were achieved by the displacement of a permanent magnet along a millimeter-sized fluidic channel, interconnecting different reservoirs. A similar method, using multiple wetting valves to allow for more complex designs, was recently presented,<sup>[11]</sup> but it still requires rather large volumes and incubation times. To increase the flexibility of these assays, Sista et al. combined this strategy with droplets manipulated on an array of electrodes by electrowetting (EWOD).<sup>[12,13]</sup> This device, generally named a digital microfluidic device, is very flexible, but it requires complex microfabrication steps to integrate the array of electrodes onto the device surface. A variant of this method, in which drops are immobilized on hydrophilic patches and droplets containing magnetic particles are magnetically actuated through microfabricated coils, was also proposed.<sup>[14]</sup> The drop size, however, is large (approximately 10  $\mu$ L) and microfabrication of the system is almost as demanding as that of the EWOD systems. Another strategy was proposed recently, in which droplets containing magnetic particles are hydrodynamically split in the presence of an asymmetric field.<sup>[15,16]</sup> This approach shares with conventional droplet microfluidic devices the possibility of processing droplets at a high throughput of tens to hundreds of drops per second. However, even if effective particle separation in a single daughter droplet is achieved, using this method for a purification process is not efficient, since the removal of the supernatant fluid is inefficient. More recently, Gu et al. attempted to induce droplet splitting in sub-nanoliter droplets by direct magnetic extraction of particles.<sup>[17]</sup> Unfortunately, in such small droplets, ferromagnetic particles were needed to reach a high enough magnetic trapping force. Because of the permanent magnetization induced in large ferromagnetic particles, resuspension of the magnetic particles after trapping was impossible, and the magnetic “plug” had to be recollected in a macroscopic tube to perform the next step (in this case PCR). Thus, on the one hand, a good separation of the magnetic particles was achieved, but on the other hand the ability to perform multiple steps was lost.


Herein, we create a device that combines these advantages. It involves a new design for magnetic capture based on programmable “magnetic tweezers”. Because of multiple trapping–release sequences, the particles can be exchanged with an extremely low carryover of supernatant (less than 2%) between droplets with volumes of 80 nL or lower. Starting from reagents contained in a microtiter plate, full automation of the method, involving several exchanges of reagents and rinsing solutions, is achieved by a combination of

[\*] Dr. A. Ali-Cherif,<sup>[†]</sup> Dr. S. Begolo,<sup>[§]</sup> Dr. S. Descroix, Dr. J.-L. Viovy, Dr. L. Malaquin  
Institut Curie UMR 168, Research Center, CNRS, UMR168  
11 rue Pierre et Marie Curie, 75005 Paris (France)  
E-mail: laurent.malaquin@curie.fr

[§] Current address: California Institute of technology  
1200 E. California Blvd. MC 101-20, Pasadena, CA 91125 (USA)

[†] These authors contributed equally to this work.

[\*\*] This work was supported in part by EU project NADINE (FP7-NMP: 246513) and by the Equipex/Idex ANR program for the IPGG project. A.A.-C. acknowledges a PhD fellowship from the French Ministry of Defense; S.B. was supported by a Curie Institute International PhD fellowship.

 Experimental details and discussion regarding modeling, droplet handling, and flow velocity effects are provided as Supporting Information, which is available on the WWW under <http://dx.doi.org/10.1002/anie.201203862>.

this new magnetic droplet device with a previously described droplet sampling strategy.<sup>[18]</sup> The working principle of bead capture and extraction is depicted in Figure 1 (see also the Supporting Information, Video SV1). The magnetic tweezers

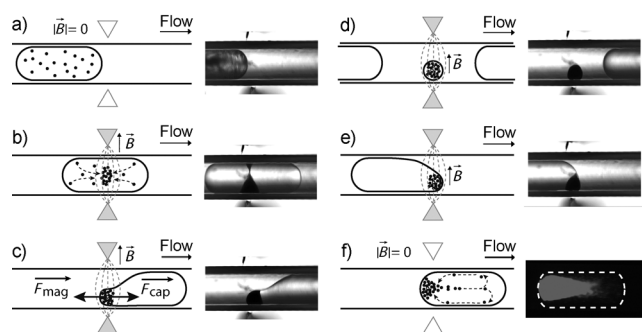


**Figure 1.** Diagram of the bead-handling steps. The capillary is inserted between magnetic tweezers: a) suspended particles, b) particle confinement, c) droplet deformation, d) bead-cluster extraction, e) beads merging into a new droplet, f) particle re-suspension. The triangles representing the magnetic tweezers are gray when activated and white when inactivated. The last image (f) was recorded with fluorescence to show the distribution of beads in the droplet.

consist of two sharp magnetic tips (AFK502 Imphy Alloys) facing each other across a microtube or hydrophobic micro-channel.<sup>[19]</sup> Depending on the configuration, each tip of the tweezers can be activated independently by a magnetic coil. A droplet containing magnetic particles is transported in the tubing by a carrier fluid at a constant flow rate around  $0.02 \mu\text{L s}^{-1}$  (see Supporting Information for discussion). As the droplet passes the magnetic tweezers, the suspended particles are attracted and form a compact cluster (Figure 1a and Supporting Information, Movie M1). When the trailing edge of the plug reaches the tweezers, the magnetic force acting on the bead-cluster deforms the droplet interface. Above a field threshold, the magnetic force overcomes the interfacial forces maintaining the droplet cohesion and a smaller particle-containing droplet is split out of the initial one (Figure 1c). The cluster droplet is kept immobile using the magnetic tweezers (Figure 1d) until the arrival of a new droplet, which spontaneously merges with it (Figure 1e). The volume of the extracted droplet is small (1 nL) as compared to the incoming droplet (80 nL), and the beads within it are essentially in a close-pack arrangement, providing a very efficient separation of the supernatant fluid (99% of the total droplet volume, see below).

After this extraction, two different actuation sequences can be used. First, the magnetic field can be maintained during the passage of one (or several) rinsing droplets. After merging, the liquid initially surrounding the particle cluster is diluted in the droplet while the particles stay confined in the magnetic trap. With this procedure, part of the residual liquid contained in the aggregate and at

its surface is further removed with the rinsing droplet(s). Second, the magnetic field can be removed after merging of a new droplet with the aggregate, to resuspend the particles (Figure 1f, Movie M1). This gives active mixing of the beads within the whole droplet owing to recirculation flows<sup>[20,21]</sup> and allows a variation of the incubation time, by adapting the flow rate and the distance between the tweezers. This method is thus well adapted to steps involving a kinetically controlled reaction at the surface of the bead (enzymatic reaction, binding, and elution).

Combining the above three functions (bead extraction, rinsing, resuspension) with the droplet-aliquoting and distribution system previously described,<sup>[18]</sup> essentially any bead-based method can be implemented, whatever its complexity. Briefly, the aliquoting system (Figure 2) involves a pipetting robot generating droplets from a microtiter plate (or any other sample container) under a double layer of oil and aqueous rinsing solution. Trains of droplets containing reagents from any of the wells can be prepared by sequential aspiration, and the size of each droplet can also be tuned independently by adapting the aspiration times. The droplet train (or a series of several droplet trains) is then pushed at constant velocity into the analysis arm with the magnetic tweezers. Herein, we describe a capillary-based method, suitable for laboratories not equipped with microfabrication facilities, but a similar system could be implemented in microfabricated channels.

Magnetic tweezers, as compared for example, to hydrodynamic bead splitting,<sup>[15,16]</sup> yields a better extraction efficiency, but it involves a more complex physical process, based on a subtle balance between magnetic, interfacial, and hydrodynamic forces. Herein, we use highly confined droplets at a constant oil flow rate, so that the hydrodynamic forces on the main droplet are larger than the two other forces. Then, the droplet can be considered within a frame of reference

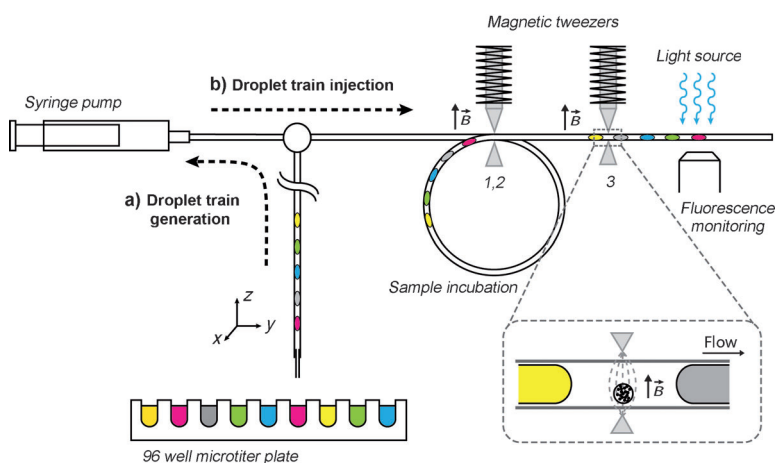


**Figure 2.** General design of the device. a) In sampling mode, a syringe pump combined with an xyz-stage and a three-way valve sequentially aspirates droplets from different wells of a microtiter plate separated by oil plugs, and stores this droplet train in the left arm of the capillary. The wells have an oil film on top to avoid evaporation and cross contamination. b) In analysis mode, this droplet train is pushed at constant speed through the system, which is two magnetic tweezers and an additional loop around the first tweezers to create two independent incubation zones.

moving at the droplet velocity, thus allowing only the balance of magnetic ( $F_m$ ) and interfacial forces ( $F_i$ ) to be evaluated (see Supporting Information for discussion). Computer simulations of the magnetic field distribution in the system were performed using COMSOL Multiphysics software, to optimize the geometry of the tweezers, perform quantitative evaluation of the magnetic field gradient in the capture area, and achieve maximal trapping force. We chose a configuration involving a pair of facing blade-like tips, with a gap adjusted to the outside diameter (OD) of the capillary, 600  $\mu\text{m}$ .

The ability to induce droplet splitting results from a balance between the magnetic forces acting on the particles in the cluster, and the force resulting from the interfacial tension, which tends to minimize surface area and thus resists droplet splitting. The conditions yielding particle extraction, that is, satisfying the condition  $F_m > F_i$ , were investigated experimentally for various induction current values, droplet velocities and magnetic particle loads (Supporting Information). A diagram corresponding to 100 nL droplets with particle load ranging between 0.1 and 1  $\mu\text{g}$  is plotted (Figure 3). Two regimes were observed: 1) a droplet splitting regime for  $F_m > F_i$ , leading to particle extraction (open

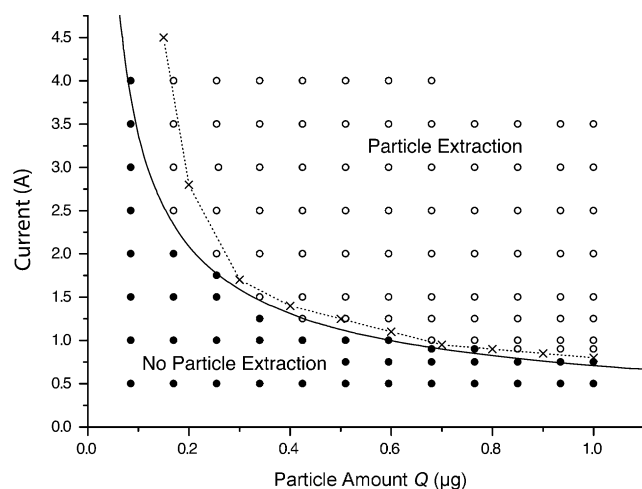


**Figure 3.** Diagram of the conditions for bead extraction (open circles), and no extraction (full circles) from the droplet as a function of current in the coil and amount of magnetic particles in one droplet  $Q$ . Crosses are numerical predictions for the transition threshold, solid line is a best fit to  $Q^{-2/3}$ .

circles), 2) a droplet disengagement regime ( $F_m < F_i$ ) in which the bead cluster is carried away in the initial droplet (full circles).

Theoretical modeling of the balance of magnetic and interfacial forces is not trivial, first because of the complex heterogeneous nature of the system, and second because there is no detailed analytical theory of dense suspensions of magnetic microparticles in high fields.<sup>[22]</sup> To predict the threshold for bead extraction as a function of current in the coil and bead content of the droplet, the values of the

magnetic flux density  $\vec{B}$  and  $\vec{\text{grad}}B$  in the device were predicted using COMSOL simulations for different current values ranging from 0.8 A to 3 A (Supporting Information, Table ST1).

Combined with the magnetization curves of the particles provided by the distributor (Supporting Information, Figure S2), magnetic forces for different particle loads were numerically calculated and compared with the interfacial force  $F_i$  (Supporting Information, Equation SE3). The predicted thresholds are plotted as crosses in Figure 3. The agreement with the experimental data is quite good, considering that no fitting parameter was used. Generally, the current threshold should follow the relation  $Q^{-2/3}$  (Supporting Information, Equation SE8) when the magnetization of the beads is saturated. This prediction is represented as the solid line, with the proportionality constant as a fitting parameter. The fit is also rather good, consistent with the numerical simulations showing that in the range of currents used herein, Dynal Myone beads are in the saturated regime (Supporting Information, Table ST1 and Figure S2). A diagram of particle extraction versus flow rate is given in Figure S4. As expected in a highly confined droplet regime, the effect of flow rate is weak.

To evaluate transfer and rinsing efficiencies, we prepared “trains” of droplets (80 nL per droplet) with the same initial load of magnetic particles (0.8  $\mu\text{g}$ ). We then transferred the content of a series of alternate drops to the subsequent one, by activating the field during the passage of a first droplet in the trap, and deactivating it during the passage of a second droplet to collect the particles extracted from the previous one (Supporting Information, Figure S3). Comparing the integrated fluorescence intensities in the initial droplets and in the droplets after extraction yielded an apparent extraction efficiency of  $98.9 \pm 0.2\%$ . This is actually an underestimation of the efficiency, because the fluorescence saturation and absorption by the iron oxide in the beads both reduce the signal from droplets containing a high number of beads.

To apply our system, we developed an immunoassay for the diagnosis of neonatal congenital hypothyroidism (CH), a disease of high prevalence (1:2000 to 1:4000 newborns), that requires analysis methods adapted to low sample volumes. The prognosis of newborns that are treated early is excellent whereas untreated CH leads to severe developmental problems. The primary clinical diagnosis of CH is based on an elevated concentration of thyroid-stimulating hormone (TSH  $> 30 \text{ mIU L}^{-1}$  serum).<sup>[23]</sup> In addition to this important clinical application, this complex method has never been fully applied in a microfluidic system. It thus provides a good proof-of-concept of the power of this method. The sandwich immunoassay used herein involves nine elementary steps (Figure 4, for clarity some steps are not shown). This system involves two magnetic tweezers (Figure 2). The first incubation is performed in a loop of tubing between the first and second passage of the capillary in front of the first tweezers, and a second incubation is performed between the first and second tweezers.

The enzymatic degradation of the substrate was monitored over time by image integration in an epifluorescence microscope equipped with a translation stage and a camera.

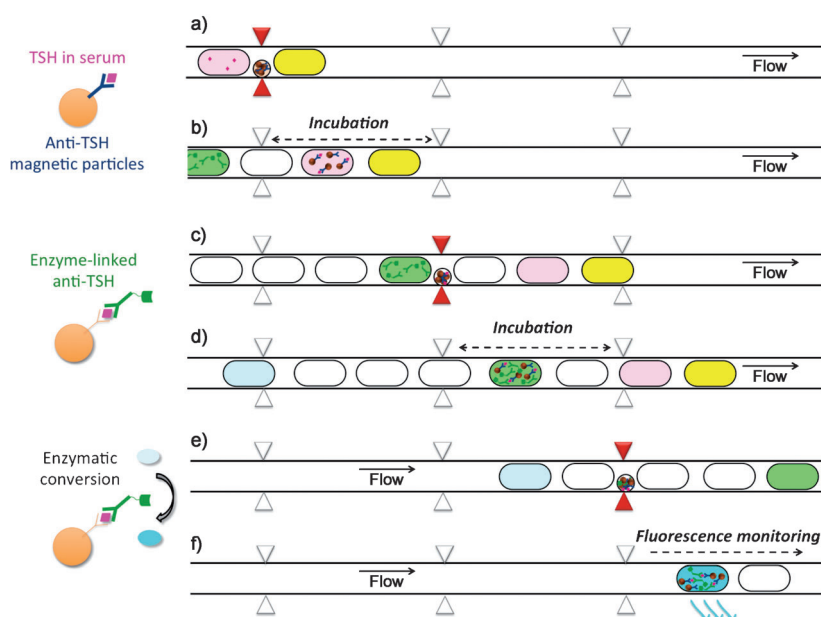


**Figure 4.** Diagram illustrating the basic steps involved in the immunoassay. Using an initial trap and resuspend sequence, antibody-bearing beads contained in the first drop were captured and transferred to a second sample drop composed of TSH in horse serum (a, b). After incubation in the capillary loop following the first tweezers, the magnetic beads with the antibody complexes were trapped again in the same tweezers and washed with a droplet of TBS buffer to remove non-specifically adsorbed proteins (c). The beads were resuspended and incubated in a fourth droplet containing the enzyme-labeled secondary antibody (d). Washing was performed in the second magnetic trap with three successive TBS droplets (e) to remove unbound secondary antibodies. Finally, the particles were released and incubated in a fluorogenic enzymatic substrate (f).

This method, also referred to as kinetic ELISA, monitors the enzyme substrate reaction kinetics. When the substrate is present in excess, a linear relationship between the enzyme concentration and the velocity of substrate turnover can be established. Kinetic ELISA was applied in microfluidic format and showed superior results to ELISA, with respect to sensitivity and robustness.<sup>[24]</sup>

The temporal evolution of the fluorescence signal within droplets with various initial TSH concentrations was investigated (Supporting Information, Figure S5). As expected, the fluorescence signal first increases linearly with time and finally reaches a plateau. The slope of the reaction curves increases with TSH concentration, giving a calibration curve for the immunoassay (Figure 5). Each point represents at least four experiments, performed on different days and raw serum samples. The relative standard deviations (RSDs) are 8–20%, with an average of 14%. The detection limit was defined as three standard deviations plus background signal,<sup>[25]</sup> 5.7 mIU L<sup>-1</sup>, corresponding to 40 pM according to the WHO 80/558 standard definition.<sup>[26]</sup> This result meets the standard of congenital hypothyroidism diagnosis, in which the typical TSH cut-off is approximately 30 mIU L<sup>-1</sup>.<sup>[23]</sup> The RSDs and sensitivity are slightly above and below those of conventional colorimetric kinetic ELISA test (10% and 2.3 mIU L<sup>-1</sup> for Immunometrics, respectively). However, our experiments were performed at room temperature (versus controlled temperature at 37°C for the Immunometrics assay), and as a first generation prototype. We thus

believe that performance comparable with or better than those of the state-of-the-art macroscopic systems can be achieved with additional engineering. Regarding speed and consumption of the assay, the whole immunoassay was performed in 10 min in less than 100 nL samples, as compared to 2.5 h and 100 µL for the Immunometrics ELISA kit.

Immunoassays were also performed in a newborn umbilical-cord plasma sample, to assess matrix effects, and confirm that the method is readily applicable to human samples. A sample composed of 8.5 mIU L<sup>-1</sup> TSH spiked into human umbilical-cord plasma was analyzed. The measured TSH level was 7.4 mIU L<sup>-1</sup>. The difference between these concentrations was 15%, and is within the error of conventional methods, acceptable for diagnosis, confirming the applicability of the method in clinical samples.

Overall, this magnetic-bead-based microfluidic platform is able to achieve purification, extraction, enzymatic reactions, and detection operations in droplets, combining high extraction efficiency (at least 99%) with programmability. Its rate of one analysis every 30 s, 120 analyses per hour, could be increased further using multiple capillaries in parallel. Moreover, as the droplet train is created using a sampling robot, analyses can

be multiplexed to screen numerous biomarkers from a single sample of tens of microliters. Finally, contamination between samples is eliminated by using fluorinated carrier oil and tubing.<sup>[27]</sup>

The kinetic ELISA detection of TSH hormone in newborn plasma yielded 40 pM sensitivity, meeting the requirements for diagnosis, with a reduction in assay time from 2.5 h to 10 min, and a reduction in sample and reagent volume per test by 1000 times. This is well beyond what is needed for diagnosis, but it should be relevant to other applications, such

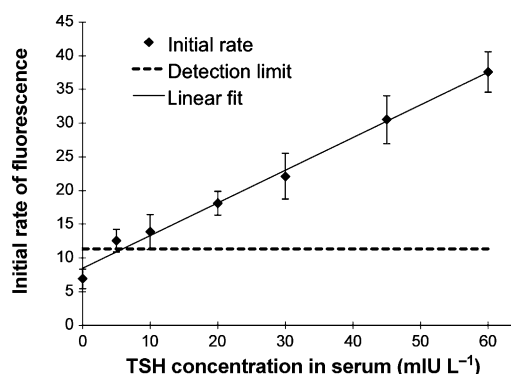


**Figure 5.** Quantitative kinetic analysis: The initial rate of fluorescence increase is plotted as a function of TSH concentration (linear part of the kinetic curves between 20 and 50 s). The detection limit is set to the background level plus three standard deviations ( $n = 5$ ).



as high-throughput low-cost screening of large libraries and proteomics. Expressed in terms of protein mass, the sensitivity obtained in 80 nL droplets represents around three attomoles, or <100 fg of protein, that is less than the typical protein content of a single cell. Also, we used a rather straightforward fluorescence detection technique and low cost camera. Using a more elaborate detector, and further reducing the droplet volume by about tenfold (which is possible, but irrelevant for our diagnostic application), we expect a gain of at least two orders of magnitude in mass sensitivity, which would allow the high-throughput detection of proteins in single eukaryotic cells. Droplet microfluidics is gaining ground in numerous areas of chemistry,<sup>[28]</sup> and our method should expand its range of applications further, opening it to heterogeneous reactions.

Received: May 18, 2012

Revised: July 4, 2012

Published online: September 26, 2012

**Keywords:** droplets · fluorescence · immunoassays · magnetic particles · microfluidics

- [1] A. B. Theberge, F. Courtois, Y. Schaerli, M. Fischleschner, C. Abell, F. Hollfelder, W. T. S. Huck, *Angew. Chem.* **2010**, *122*, 5982; *Angew. Chem. Int. Ed.* **2010**, *49*, 5846.
- [2] J. J. Agresti, E. Antipov, A. R. Abate, K. Ahn, A. C. Rowat, J.-C. Baret, M. Marquez, A. M. Klibanov, A. D. Griffiths, D. A. Weitz, *Proc. Natl. Acad. Sci. USA* **2010**, *107*, 4004.
- [3] M. Chabert, K. D. Dorfman, J.-L. Viovy, *Electrophoresis* **2005**, *26*, 3706.
- [4] M. Chabert, J.-L. Viovy, *Proc. Natl. Acad. Sci. USA* **2008**, *105*, 3191.
- [5] J. F. Edd, D. Di Carlo, K. J. Humphry, S. Köster, D. Irimia, D. A. Weitz, M. Toner, *Lab Chip* **2008**, *8*, 1262.
- [6] C. Baroud, F. Gallaire, R. Dangla, *Lab Chip* **2010**, *10*, 2032.
- [7] T. Thorsen, S. J. Maerkl, S. R. Quake, *Science* **2002**, *298*, 580.
- [8] A. Le Nel, N. Minc, C. Smadja, M. Slovakova, Z. Bilkova, J.-M. Peyrin, J.-L. Viovy, M. Taverna, *Lab Chip* **2008**, *8*, 294.
- [9] A.-E. Saliba, L. Saias, E. Psychari, N. Minc, D. Simon, F.-C. Bidard, C. Mathiot, J.-Y. Pierga, V. Fraissier, J. Salamero, V. Saada, F. Farace, P. Vielh, L. Malaquin, J.-L. Viovy, *Proc. Natl. Acad. Sci. USA* **2010**, *107*, 14524.
- [10] M. Shikida, K. Takayanagi, K. Inouchi, H. Honda, K. Sato, *Sens. Actuators B* **2006**, *113*, 563.
- [11] S. M. Berry, L. J. Maccoux, D. Beebe, *Anal. Chem.* **2012**, DOI: 10.1021/ac300085m.
- [12] R. Sista, Z. Hua, P. Thwar, A. Sudarsan, V. Srinivasan, A. Eckhardt, M. Pollack, V. Pamula, *Lab Chip* **2008**, *8*, 2091.
- [13] R. S. Sista, A. E. Eckhardt, V. Srinivasan, M. G. Pollack, S. Palanki, V. K. Pamula, *Lab Chip* **2008**, *8*, 2188.
- [14] U. Lehmann, C. Vandevyver, V. K. Parashar, M. A. M. Gijs, *Angew. Chem.* **2006**, *118*, 3132; *Angew. Chem. Int. Ed.* **2006**, *45*, 3062.
- [15] D. Lombardi, P. S. Dittrich, *Anal. Bioanal. Chem.* **2011**, *399*, 347.
- [16] E. Alhetlani, O. J. Hatt, M. Vojtisek, M. D. Tarn, N. Pamme, *µTAS Proceedings* **2010**, 1817.
- [17] S.-Q. Gu, Y.-X. Zhang, Y. Zhu, W.-b. Du, B. Yao, Q. Fang, *Anal. Chem.* **2011**, *83*, 7570–7576.
- [18] M. Chabert, K. D. Dorfman, P. de Cremoux, J. Roeraade, J.-L. Viovy, *Anal. Chem.* **2006**, *78*, 7722.
- [19] S. Begolo, G. Colas, J. L. Viovy, L. Malaquin, *Lab Chip* **2011**, *11*, 508.
- [20] H. Song, J. D. Tice, R. F. Ismagilov, *Angew. Chem.* **2003**, *115*, 792; *Angew. Chem. Int. Ed.* **2003**, *42*, 768.
- [21] S. R. Hodges, O. E. Jensen, J. M. Rallison, *J. Fluid Mech.* **2004**, *501*, 279.
- [22] M. Shikida, K. Takayanagi, H. Honda, H. Ito, K. Sato, *J. Micromech. Microeng.* **2006**, *16*, 1875.
- [23] M. V. Rastogi, S. H. Lafranchi, *Orphanet J. Rare Dis.* **2010**, *5*, 1.
- [24] N. Yanagisawa, D. Dutta, *Biosensors* **2011**, *1*, 58.
- [25] *Immunoassay* (Eds.: E. P. Diamandis, T. K. Christopoulos), Academic Press, San Diego, **1996**.
- [26] R. E. Gaines Das, A. F. Bristow, *J. Endocrinol.* **1985**, *104*, 367.
- [27] K. D. Dorfman, M. Chabert, J.-H. Codarbox, G. Rousseau, P. de Cremoux, J.-L. Viovy, *Anal. Chem.* **2005**, *77*, 3700.
- [28] H. Song, D. L. Chen, R. F. Ismagilov, *Angew. Chem.* **2006**, *118*, 7494; *Angew. Chem. Int. Ed.* **2006**, *45*, 7336.